

Supporting Information

Symmetric Poly(ethylene oxide-*b*-styrene-*b*-isoprene) Triblock Copolymers: Synthesis, Characterization and Self-Assembly in Bulk and Thin Film

Yali Qiao,[†] Rachel Ferebee,[§] Bongjoon Lee,[§] Indranil Mitra,[#] Nathaniel A. Lynd,[‡] Jeffery Hayat,[†] Gila E. Stein,^{#*} Michael R. Bockstaller^{§*} and Chuanbing Tang^{†*}

[†]Department of Chemistry and Biochemistry, University of South Carolina, Columbia, South Carolina 29208, USA

[§]Department of Materials Science and Engineering, Carnegie Mellon University, Pittsburgh, Pennsylvania 15213, USA

[#]Department of Chemical & Biomolecular Engineering, University of Houston, Houston, Texas 77204, USA

[‡]Materials Sciences Division, Lawrence Berkeley National Laboratory, Berkeley, California 94720, USA

Corresponding Author E-mail: tang4@mailbox.sc.edu; bockstaller@cmu.edu; gestein@uh.edu

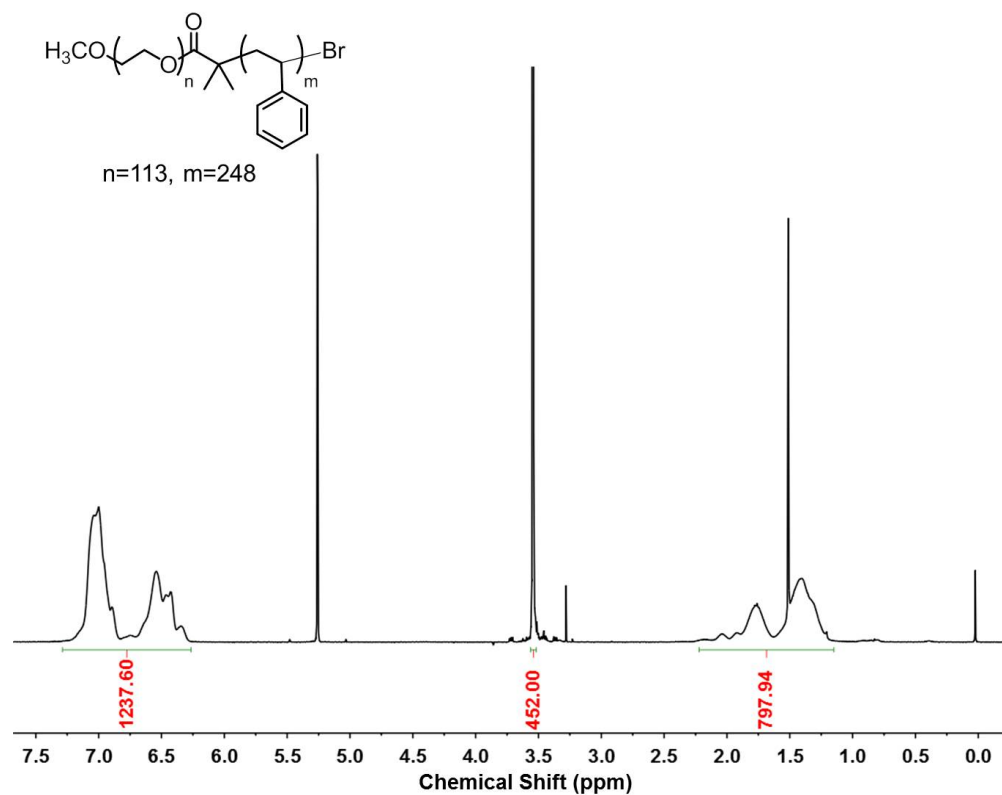


Figure S1. Representative ^1H NMR spectrum of PEO-PS-Br in CDCl_3 .

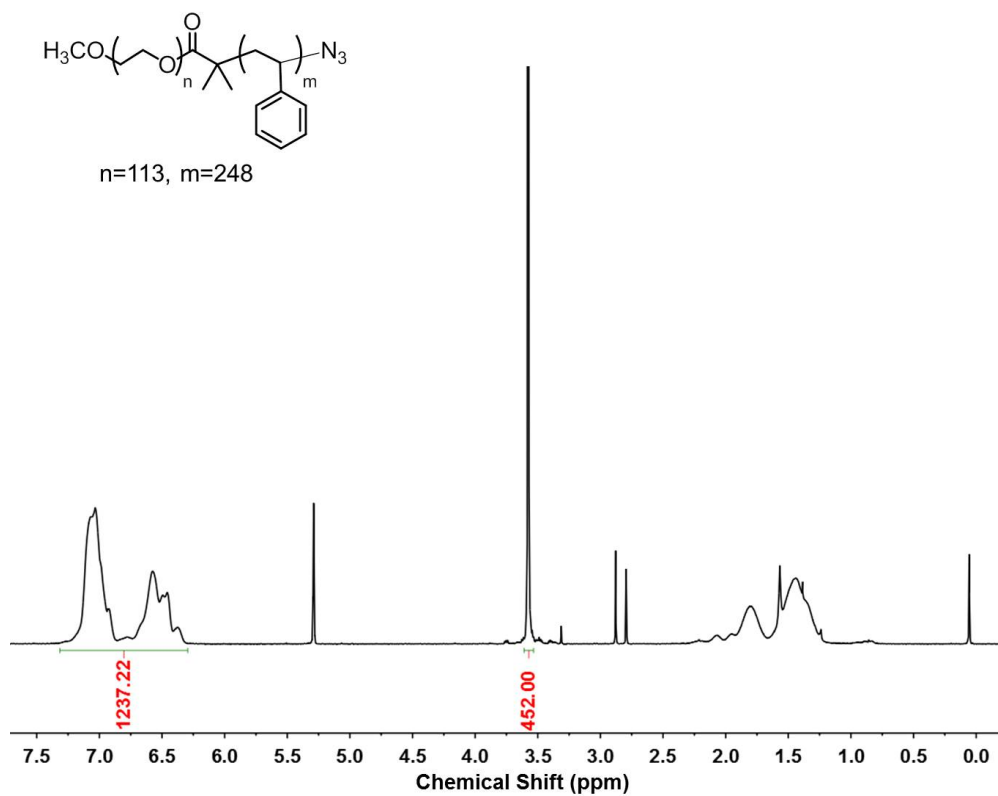


Figure S2. Representative ^1H NMR spectrum of PEO-PS- N_3 in CDCl_3 .

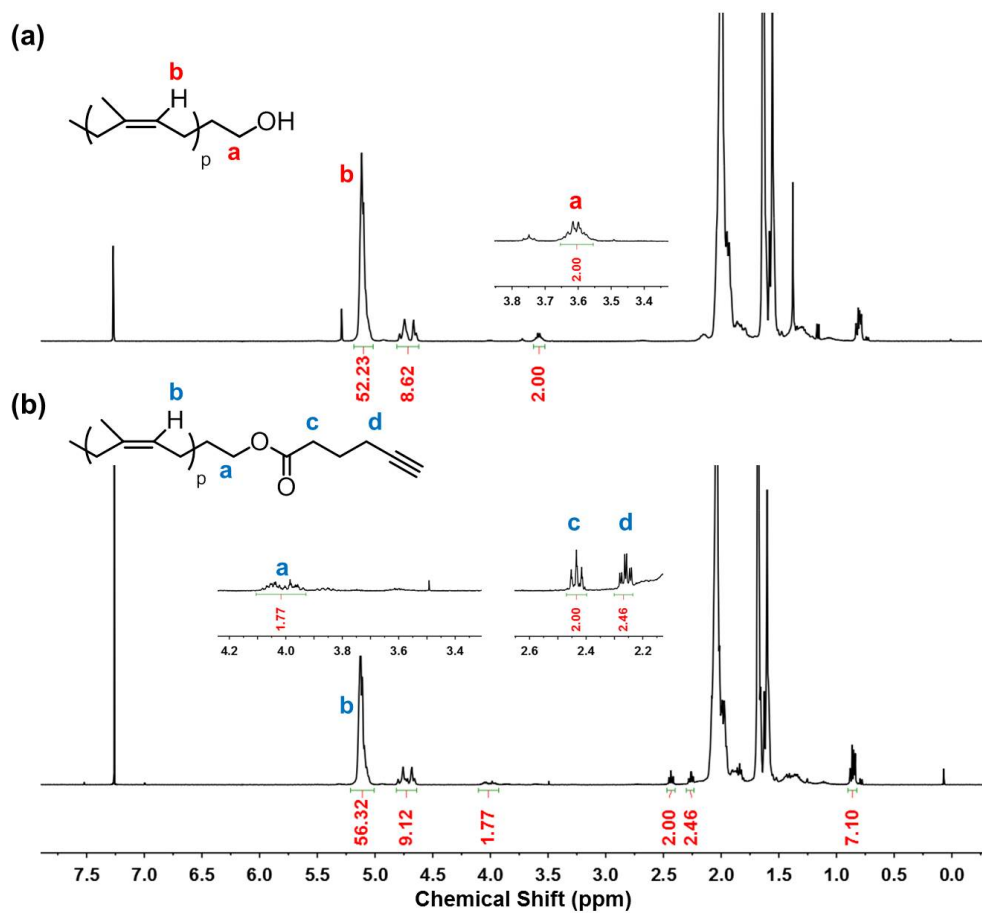


Figure S3. ^1H NMR spectra of alkyne-functionalized PI and hydroxyl-terminated PI in CDCl_3 .

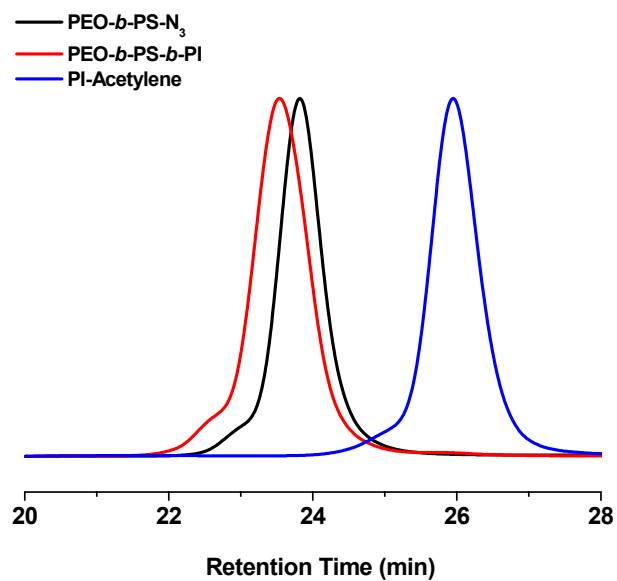


Figure S4. GPC traces following the synthesis of PEO-PS-PI triblock copolymer

(OS12) in THF.

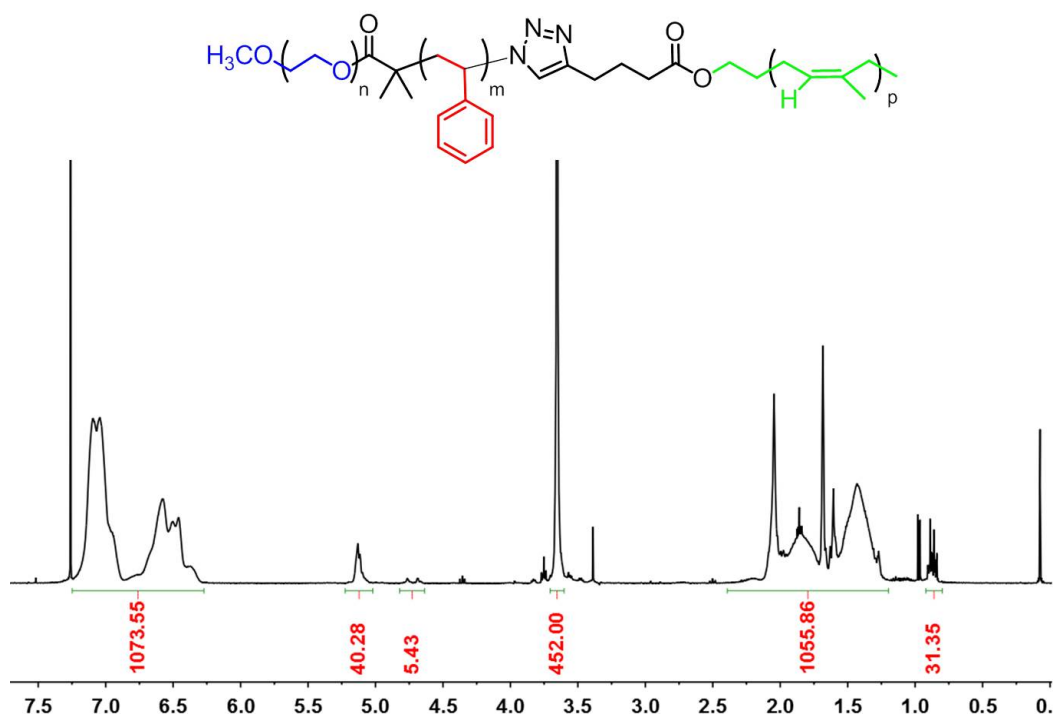


Figure S5. ¹H NMR spectrum of PEO-PS-PI triblock copolymer (OS12) in CDCl₃.

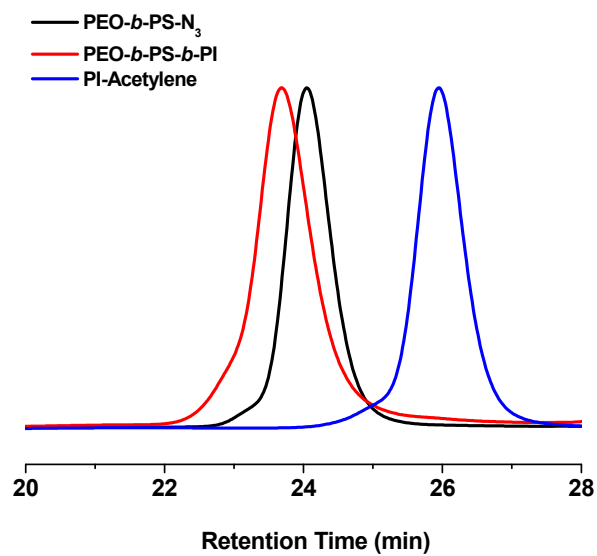


Figure S6. GPC traces following the synthesis of PEO-PS-PI triblock copolymer (OS11) in THF.

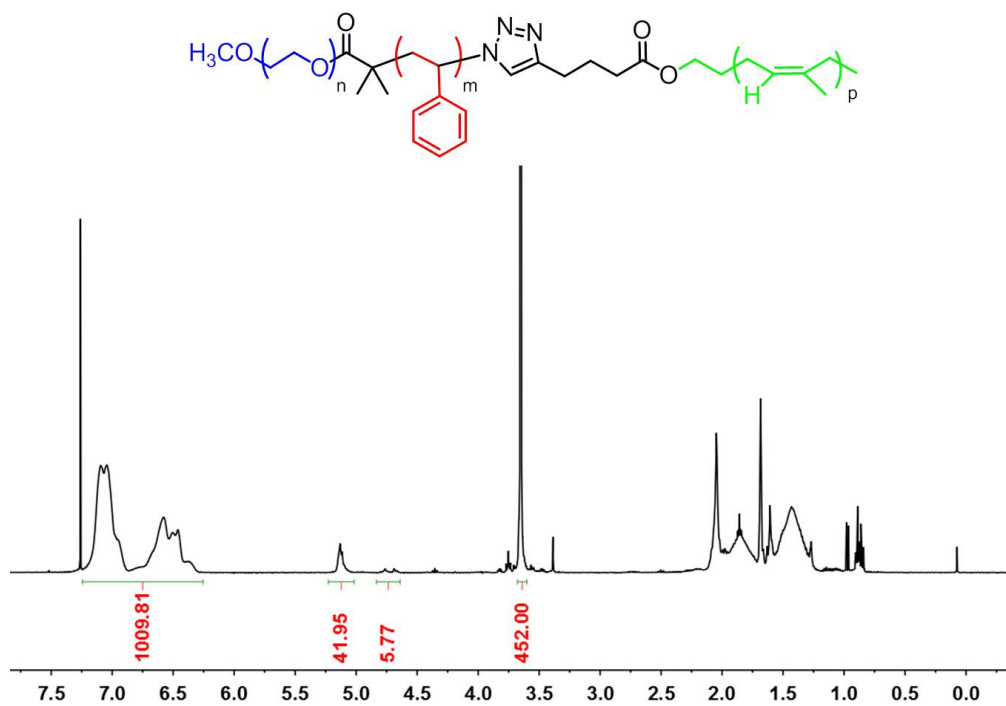


Figure S7. ¹H NMR spectrum of PEO-PS-PI triblock copolymer (**OSI1**) in CDCl₃.

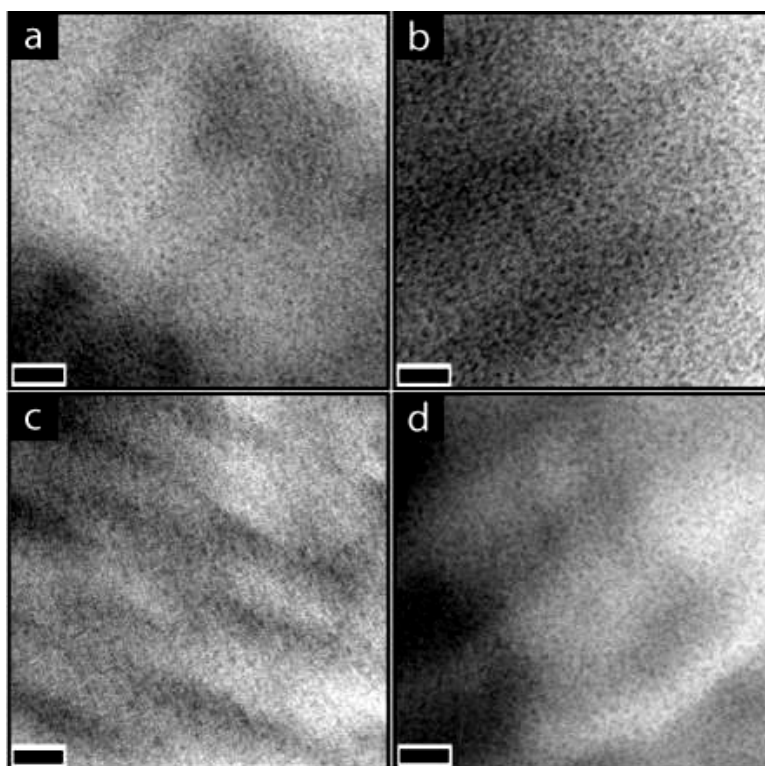


Figure S8. TEM images of **OSI1** (a) as cast, (c) 72 h thermal annealing at *T* = 120 °C; and **OSI3** (b) as cast, (d) 72 h thermal annealing at *T* = 120 °C. (scale bar = 50 nm)

Grazing-Incidence Small Angle X-ray Scattering (GISAXS): The following paragraphs describe our attempts to characterize the out-of-plane order in thin films of OSI triblocks (high-humidity solvent annealing, with and without LiCl electrolyte). The first sample considered is “no salt.” The GISAXS intensity from this sample was not very strong, so there is only one peak that shows any out-of-plane structure (at $q_y = 0.23 \text{ nm}^{-1}$). The out-of-plane intensity $I(q_z)$ for this peak is displayed in **Figure S9**, where the raw data are displayed as red dots, and simulated profiles based on the DWBA are shown as solid black lines. The simulations assumed (a) FCO spheres; (b) FCC spheres; (c) HCP spheres; (d) Monolayer of hexagonal spheres; and (e) Perpendicular cylinders with in-plane hexagonal symmetry. Of the first three spherical-domain symmetries considered in **Figure S9**, the FCO symmetry is closest to the experimental data, although FCC and HCP are also qualitatively consistent. The predicted scattering for a monolayer of spheres fails to capture any of the out-of-plane structure. The predicted scattering for perpendicular cylinders can capture the out-of-plane oscillation period, so this model might seem appropriate. We address this point further in the following paragraph, but it is important to note that a humidity-induced transition to cylinders is not anticipated, and the measured nearest-neighbor distance is very close to the bulk BCC value.

The next sample considered is the low salt concentration ($[\text{O}]:[\text{Li}^+] = 16:1$). We compare measured and simulated GISAXS patterns for out-of-plane line cuts at $q_y = 0.28 \text{ nm}^{-1}$, 0.32 nm^{-1} , and 0.42 nm^{-1} . **Figure S10** (part a) shows predictions for perpendicular cylinders. The form factor for perpendicular cylinders generates periodic fringes along the q_z axis that are in-phase along the q_y axis. However, the experimental fringes are clearly out-of-phase along the q_y axis, so we do not believe that swelling of PEO (by humidity, or humidity and LiCl) will induce a phase transition from spherical to cylindrical morphology. The remainder of this analysis is therefore restricted to spherical-domain symmetries. Figure S10 also includes predictions for (b) FCO spheres; (c) FCC spheres; and (d) HCP spheres. None of these models can capture the out-of-plane structure at $q_y = 0.28 \text{ nm}^{-1}$, which is nearly

featureless, but HCP is consistent with the $I(q_z)$ profiles at 0.32 nm^{-1} and 0.42 nm^{-1} .

The final sample discussed in this manuscript has the highest salt content ($[\text{O}]:[\text{Li}^+] = 8:1$). We compare measured and simulated GISAXS patterns for out-of-plane line cuts at $q_y = 0.28 \text{ nm}^{-1}$, 0.32 nm^{-1} , and 0.42 nm^{-1} . **Figure S11** shows predictions for (a) FCO spheres; and (b) FCC spheres. HCP symmetry was a poor match and is not shown here. FCC predictions are qualitatively consistent with the data. However, the data at all values of q_y are significantly “smeared” along the q_z axis, so it is difficult to refine the model.

The actual structure in all films is probably more complex than a well-defined FCO, FCC, or HCP symmetry, so the simulations will never offer quantitative agreement with data. The kinetically-controlled morphology could include more than one stacking sequence, which may be a response to local variations in film thickness (a common occurrence with solvent annealed films, and confirmed for these samples with optical microscopy).

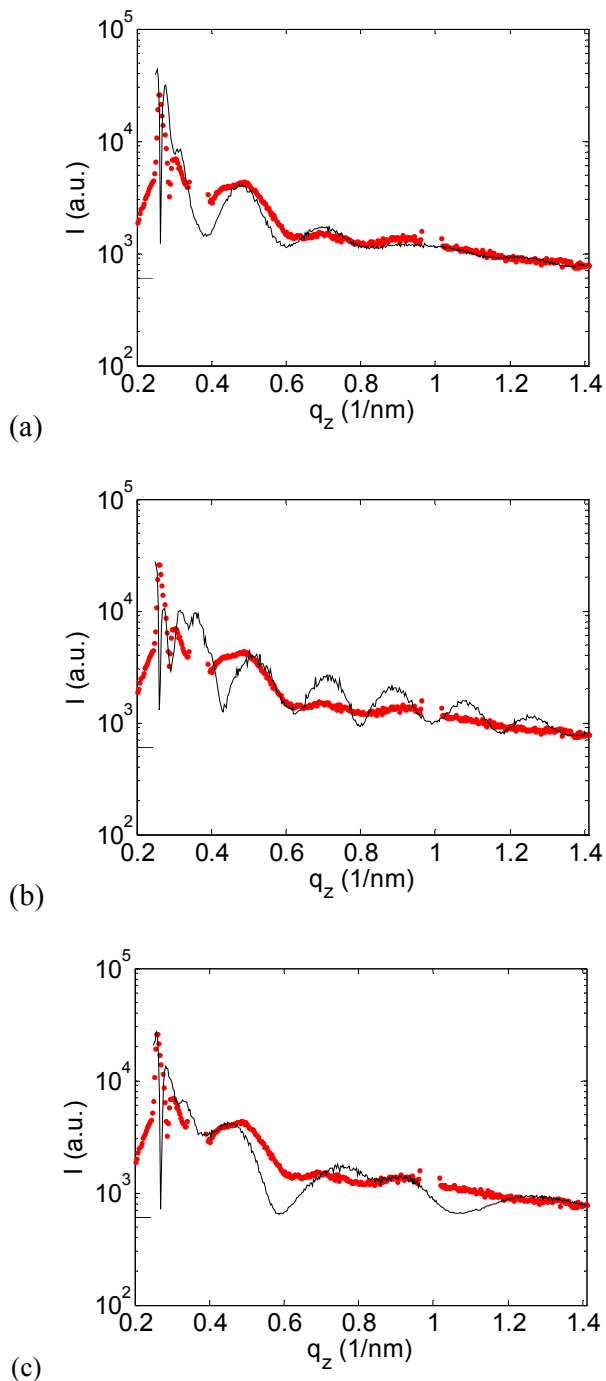


Figure S9: No salt film. GISAXS intensity along the out-of-plane axis at $q_y = 0.23 \text{ nm}^{-1}$. Solid black line is the predicted intensity based on the DWBA with the following assumptions: (a) FCO stacking of three layers, with layer thickness = $(14 \pm 3) \text{ nm}$, sphere diameter = $(10 \pm 2) \text{ nm}$. (b) FCC stacking of three layers, with layer thickness = $(17 \pm 3) \text{ nm}$, sphere diameter = $(10 \pm 2) \text{ nm}$. (c) HCP stacking of three layers, with layer thickness = $(14 \pm 3) \text{ nm}$, sphere diameter = $(10 \pm 2) \text{ nm}$.

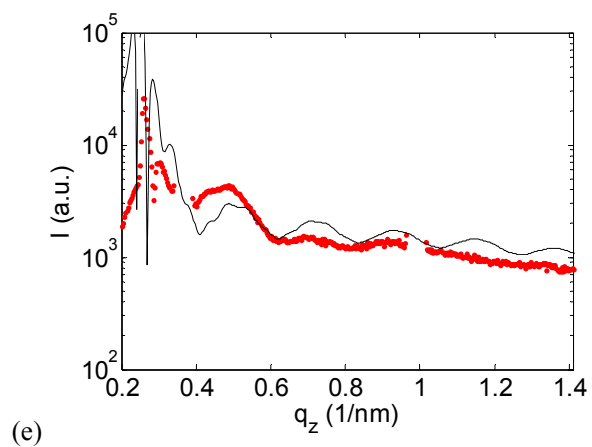
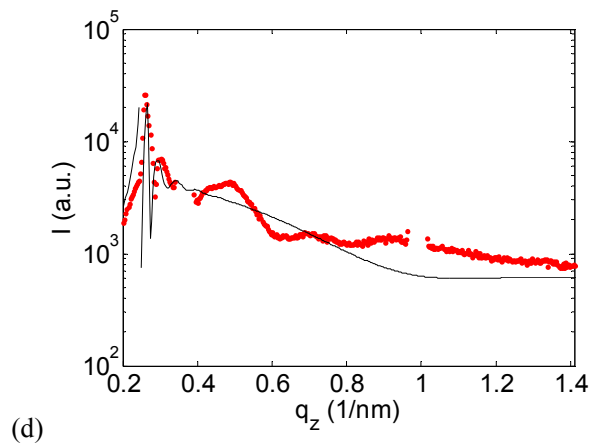


Figure S9: No salt film, continued. GISAXS intensity along the out-of-plane axis at $q_y = 0.23 \text{ nm}^{-1}$. Solid black line is the predicted intensity based on the DWBA with the following assumptions: (d) Monolayer of spheres, sphere diameter = $(10 \pm 2) \text{ nm}$. (e) Perpendicular cylinders, cylinder diameter = $(10 \pm 2) \text{ nm}$, cylinder height = 30 nm .

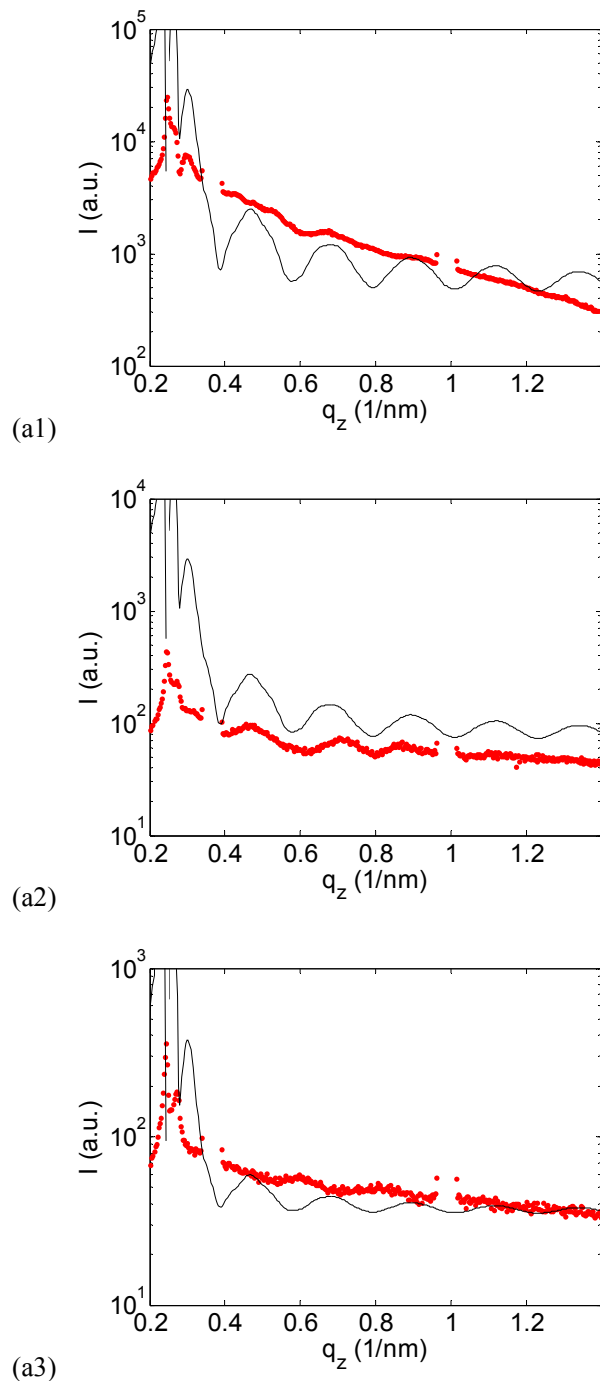


Figure S10: Low salt concentration ($[\text{O}]:[\text{Li}^+] = 16:1$). GISAXS intensity along the out-of-plane axis at (a1) $q_y = 0.28 \text{ nm}^{-1}$; (a2) $q_y = 0.32 \text{ nm}^{-1}$; and (a3) $q_y = 0.42 \text{ nm}^{-1}$. Solid black line is the predicted intensity based on the DWBA with the following assumptions: Perpendicular cylinders with diameter = $(10 \pm 2) \text{ nm}$ and height = 28 nm .

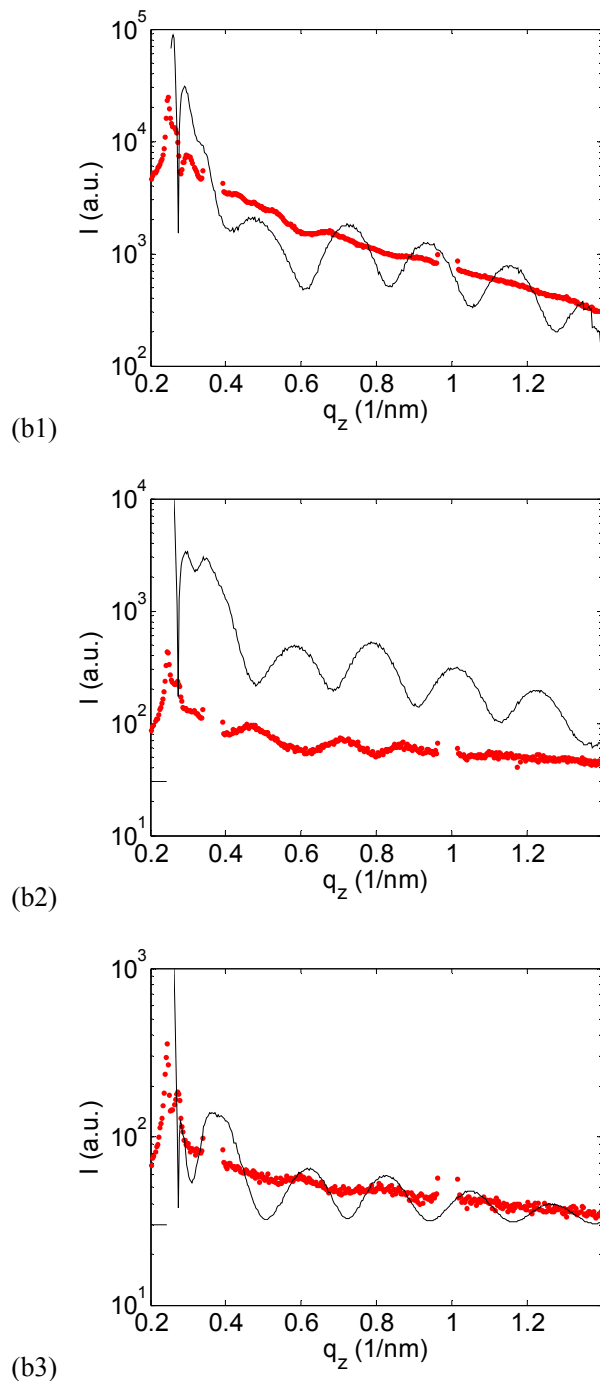


Figure S10: Low salt concentration ($[\text{O}]:[\text{Li}^+] = 16:1$), continued. GISAXS intensity along the out-of-plane axis at (b1) $q_y = 0.28 \text{ nm}^{-1}$; (b2) $q_y = 0.32 \text{ nm}^{-1}$; and (b3) $q_y = 0.42 \text{ nm}^{-1}$. Solid black line is the predicted intensity based on the DWBA with the following assumptions: FCO stacking of two layers, with layer thickness = $(28 \pm 3) \text{ nm}$, sphere diameter = $(18 \pm 2) \text{ nm}$.

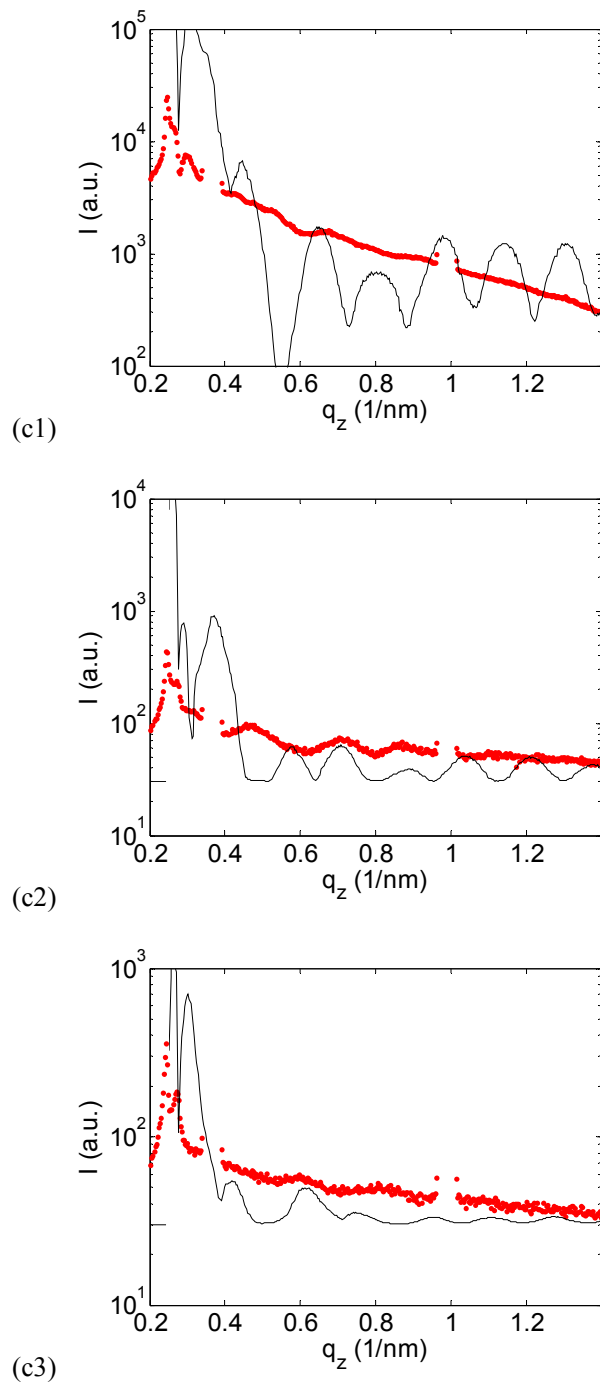


Figure S10: Low salt concentration ($[\text{O}]:[\text{Li}^+] = 16:1$), continued. GISAXS intensity along the out-of-plane axis at (c1) $q_y = 0.28 \text{ nm}^{-1}$; (c2) $q_y = 0.32 \text{ nm}^{-1}$; and (c3) $q_y = 0.42 \text{ nm}^{-1}$. Solid black line is the predicted intensity based on the DWBA with the following assumptions: FCC stacking of three layers, with layer thickness = $(19 \pm 3) \text{ nm}$, sphere diameter = $(18 \pm 2) \text{ nm}$.

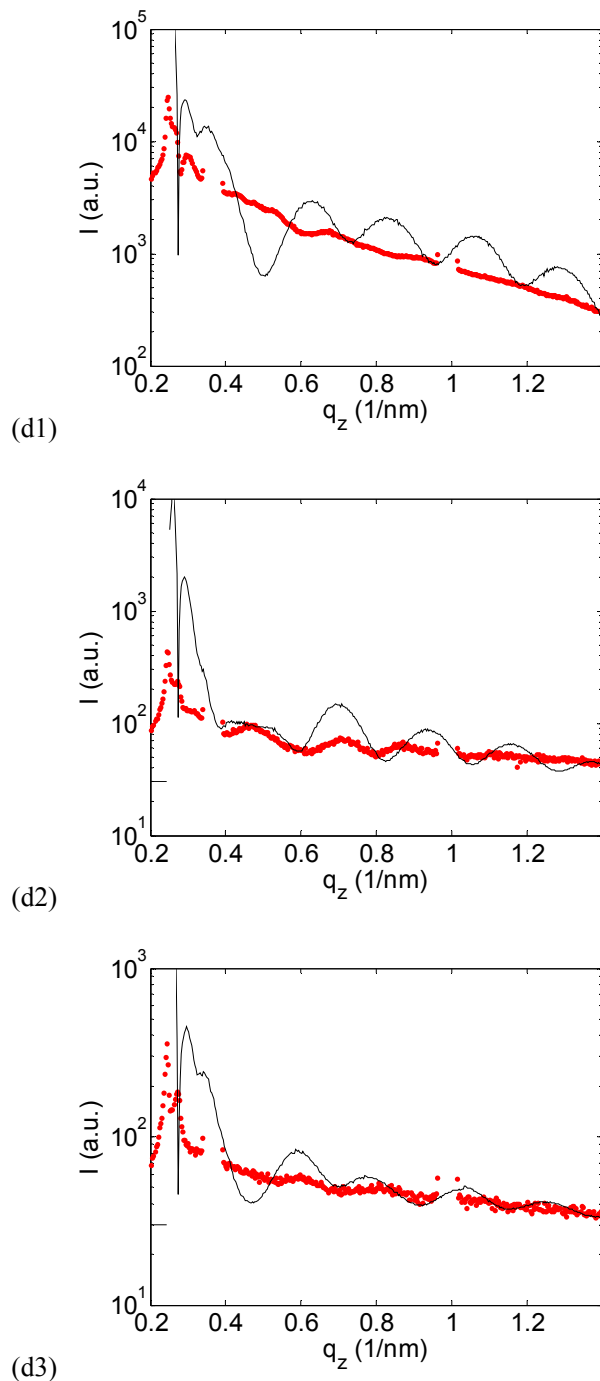


Figure S10: Low salt concentration ($[\text{O}]:[\text{Li}^+] = 16:1$), continued. GISAXS intensity along the out-of-plane axis at (d1) $q_y = 0.28 \text{ nm}^{-1}$; (d2) $q_y = 0.32 \text{ nm}^{-1}$; and (d3) $q_y = 0.42 \text{ nm}^{-1}$. Solid black line is the predicted intensity based on the DWBA with the following assumptions: HCP stacking of two layers, with layer thickness = $(27 \pm 3) \text{ nm}$, sphere diameter = $(18 \pm 2) \text{ nm}$.

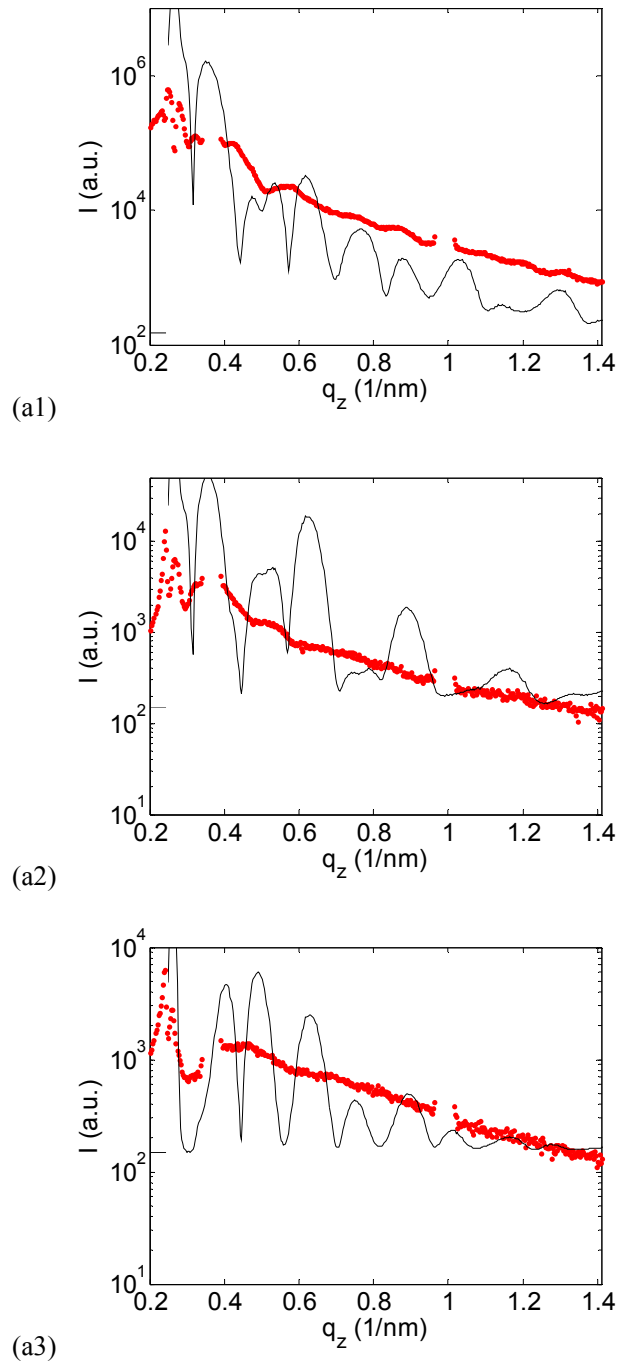


Figure S11: High salt concentration ($[O]:[Li^+] = 8:1$). GISAXS intensity along the out-of-plane axis at (a1) $q_y = 0.28 \text{ nm}^{-1}$; (a2) $q_y = 0.32 \text{ nm}^{-1}$; and (a3) $q_y = 0.42 \text{ nm}^{-1}$. Solid black line is the predicted intensity based on the DWBA with the following assumptions: FCO stacking of three layers, with layer thickness = $(25 \pm 3) \text{ nm}$, sphere diameter = $(23 \pm 4) \text{ nm}$.

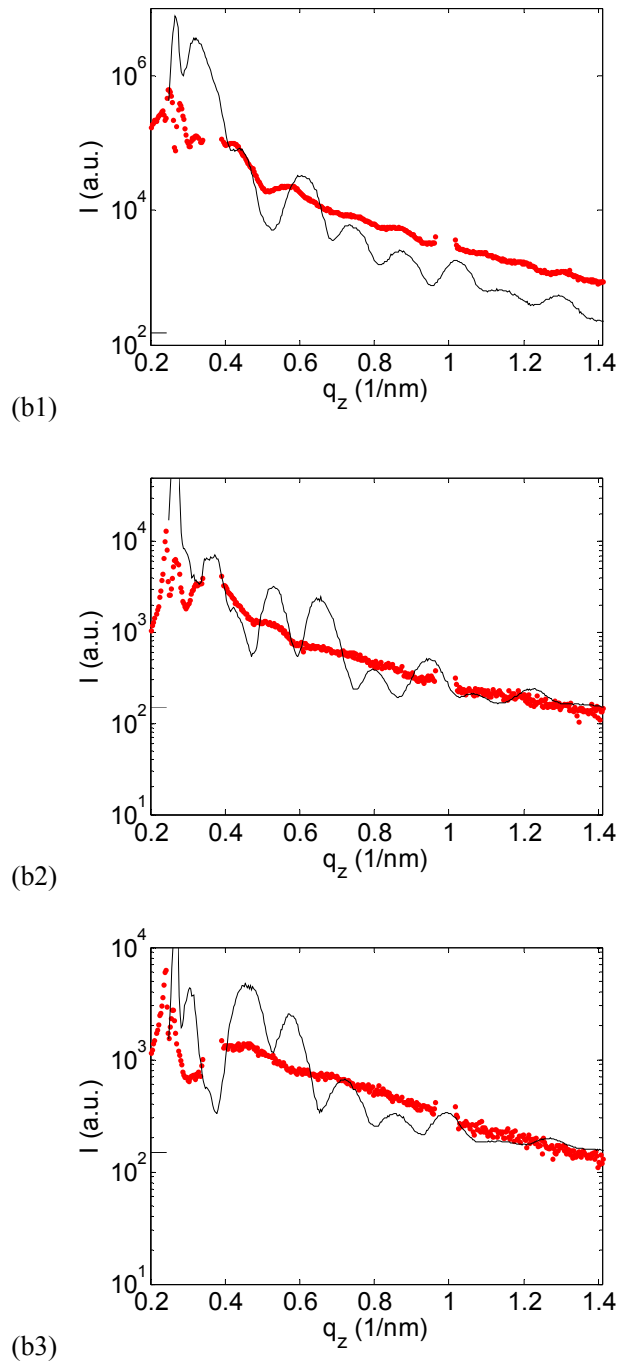


Figure S11: High salt concentration ($[O]:[Li^+] = 8:1$). GISAXS intensity along the out-of-plane axis at (b1) $q_y = 0.28 \text{ nm}^{-1}$; (b2) $q_y = 0.32 \text{ nm}^{-1}$; and (b3) $q_y = 0.42 \text{ nm}^{-1}$. Solid black line is the predicted intensity based on the DWBA with the following assumptions: FCC stacking of three layers, with layer thickness = $(23 \pm 3) \text{ nm}$, sphere diameter = $(23 \pm 4) \text{ nm}$.